Available online at www.sciencedirect.com
ScienceDirect
Procedia Engineering 2 (2010) 2085–2094
Procedia Engineering
www.elsevier.com/locate/procedia

Fatigue 2010

Effect of austenite stability on the low cycle fatigue behavior and microstructure of high alloyed metastable austenitic cast TRIP-steels

A. Glage*, A. Weidner, H. Biermann

Institute for Materials Engineering, Technische Universität Bergakademie Freiberg, Gustav-Zeuner-Strasse 5, 09596 Freiberg, Germany

Received 2 March 2010; revised 10 March 2010; accepted 15 March 2010

Abstract

Room-temperature total strain controlled low-cycle fatigue tests were carried out on two types of high alloyed metastable austenitic cast TRIP steels with different chemical compositions resulting in different austenite stabilities. The cyclic stress response revealed combinations of cyclic hardening, saturation and cyclic softening, depending on the applied total strain amplitude. In the case of the more metastable TRIP steel a considerable amount of deformation-induced α'-martensite is responsible for a high degree of cyclic hardening. Conversely, the more stable TRIP steel shows also a high degree of hardening without a significant transformation of austenite into α'-martensite, however at significantly higher strain amplitudes. The deformation-induced α'-martensite was detected in situ with a feritscope sensor. EBSD measurements were performed to investigate the locations where the phase transformation from austenite to martensite takes place. It was observed that the martensitic transformation occurs preferentially inside deformation bands. The deformation microstructures were characterized by scanning electron microscopy. Dislocation structures were studied by ECCI (electron channelling contrast imaging). Planar and well developed cell/wall structures were observed, depending on the applied total strain amplitude.

Keywords: LCF; TRIP steels; TWIP steels; Deformation-induced martensite formation

1. Introduction

Recently, a high alloying concept for cast CrMnNi TRIP steels was developed in order to achieve exceptional mechanical properties in terms of high specific strength and high ductility [1-3]. In this group of cast steels, nickel is partially replaced by other austenite stabilizing elements, e.g. manganese and nitrogen. In the last years, a pronounced production increase of related steel grades (AISI 200 series) has been recognized due to the rising nickel price [4]. Such steels and cast steels show the twinning-induced plasticity (TWIP) and transformation-induced plasticity (TRIP) effect, depending on chemical composition and temperature. The occurring deformation mechanisms are closely related to the stacking fault energy (SFE) of the austenitic structure [5]. Frommeyer et al. [6] stated that at a SFE lower than 16 mJ/m² the γ-ε-transformation is the favored mechanism, whereas a SFE above 25 mJ/m² sup-

* Corresponding author. Tel.:+49 371 39 2124; fax: +49 3731 39 3703.
E-mail address: glage@ww.tu-freiberg.de

1877-7058
doi:10.1016/j.proeng.2010.03.224

ports the twinning mechanism and above 60 mJ/m² dislocation gliding. The SFE depends on the chemical composition and temperature and can be estimated by the following semi-empirical relation [7]:

$$SFE\ [mJ/m^2] = 25.7 + 2 \cdot Ni + 410 \cdot C - 0.9 \cdot Cr - 77 \cdot N - 13 \cdot Si - 1.2 \cdot Mn \quad (1)$$

Moreover, the chemical composition has a fundamental influence on the austenite phase stability [8]. The parameters commonly used to express the austenite stability are the martensite start temperature, M_s and the M_{d30}-temperature, which represents the lowest temperature where 50 % of deformation-induced α'-martensite is formed with a true strain of 30%. Obviously, the lower the parameters are, the greater will be the respective austenite stability. Two of the frequently used equations for estimating the values of M_s and M_{d30} are [9]:

$$M_s\ [°C] = 1350 - 1665 \cdot (C+N) - 28 \cdot Si - 33 \cdot Mn - 42 \cdot Cr - 61 \cdot Ni \quad (2)$$

$$M_{d30}\ [°C] = 413 - 462 \cdot (C+N) - 9.2 \cdot Si - 8.1 \cdot Mn - 13.7 \cdot Cr - 9.5 \cdot Ni - 18.5 \cdot Cr \quad (3)$$

The mechanical behavior of metastable austenitic stainless steels, such as AISI 201, 304 and 321 has been investigated very well and considerable literature is available about the deformation-induced martensitic transformation under monotonic [10-12] and cyclic loading [13-26]. By performing strain-controlled fatigue tests, it has been shown that the martensitic transformation results in a fatigue life reduction in the LCF regime, whereas the HCF behavior is beneficially influenced. The decrease of the fatigue life in the LCF regime is attributed to the increase of the stress amplitude due to the martensitic transformation. Moreover, it is expected that the martensite acts as a preferential crack initiation site. The positive effects in the HCF regime are associated with the nucleation of very fine martensite particles in the area of local plasticity, which hinders the dislocation motion [24]. Moreover, it has been shown that a certain plastic strain amplitude $\Delta\varepsilon_p/2$ and a certain threshold value of the cumulative plastic strain must be exceeded to trigger the martensitic transformation [13,24]. The threshold value of the cumulative plastic strain increases with decreasing plastic strain amplitude, since the defect density decreases and defects such as deformation twins, stacking faults and ε-martensite are the effective nucleation sites of the α'-martensite [13,14,25].
In a previous work [23], we already analyzed the cyclic deformation behavior of the more stable cast steel 16Cr-7Mn-8Ni. For a better structural reliability it is important to assess the effect of the austenite stability on the LCF behavior. Thus, the present investigation is performed to study the influence of the austenite stability on the cyclic deformation behavior, microstructures and phase transformations.

2. Experimental details

The materials used in this study are two high alloyed austenitic stainless cast steels, denoted as 16-7-8 and 16-6-6 (nominal concentration in wt.-% Cr-Mn-Ni), cast by ACTech, Freiberg, Germany. The chemical compositions, SFE as well as the parameters for determination the austenite stability are given in Table 1. Obviously, the higher amount of nickel and manganese in the alloy 16-7-8 results in a higher austenite stability. Moreover, the calculated SFE values argue that twinning is the favored deformation mechanism in the steel 16-7-8, whereas the steel 16-6-6 should have a higher tendency to form the hexagonal ε-martensite. The supplied plates were subjected to solution annealing treatments at 1050°C for 1/2 hour followed by water quenching. From these plates, smooth cylindrical fatigue test specimens were machined with a gauge diameter of 8 mm and a gauge length of 14 mm. Prior to fatigue testing all specimens were carefully electrolytically polished in order to minimize the surface effect on the fatigue properties and to remove the martensitic surface layer produced during machining.
Low cycle fatigue tests were performed at room temperature under total strain control on a 100 kN servohydraulic testing system (MTS 810) using triangular load-time functions. The total strain amplitude $\Delta\varepsilon_t/2$ was varied between $0.1 \cdot 10^{-2}$ and $3 \cdot 10^{-2}$ at a constant strain ratio of R_ε=-1 and constant strain rate of $4 \cdot 10^{-3}$ s^{-1}. Depending on the strain amplitude the test frequency was adjusted using the relationship: $f = \dot{\varepsilon} / (4 \cdot \Delta\varepsilon_t/2)$.

Table 1. Chemical compositions and stability parameters of the investigated TRIP/TWIP cast steels.

Alloy	C	Cr	Mn	Ni	Si	Al	N	SFE [mJ/m²] (Eq. 1)	M_s [°C] (Eq. 2)	M_{d30} [°C] (Eq. 3)
16-7-8	0.07	15.91	6.58	7.65	0.85	0.07	0.07	31	-264	-4
16-6-6	0.06	15.20	5.46	5.70	0.96	0.09	0.06	26	-26	47

A clip-on extensometer was applied to measure the strain and the tests were performed until the specimens failed. Specimen failure was determined by a drop in tensile load of 5 %. A feritscope (Helmut Fischer GmbH, Fischerscope MMS PC) was used for the quantification of the ferromagnetic α'-martensite phase. The device was calibrated with δ-ferrite standard samples of known ferrite content and the results were converted to the α'-martensite contents with the correlation factor of 1.7 [27]. The effect of the specimen shape on the results was compensated by means of a correction curve provided by the manufacturer of the device (Helmut Fischer GmbH and TU Kaiserslautern). The samples for optical microscopy (OM) and scanning electron microscopy (SEM) were sectioned parallel to the loading axis and were carefully prepared by grinding and final electropolishing. For OM investigations specimens were etched in Beraha II solution. The microstructure was characterized using a FE-SEM (LEO 1530), equipped with a retractable four-quadrant BSE (backscattered electron) detector. Furthermore, this microscope was equipped with an additional high-current mode allowing the visualization of dislocation structures by using the ECCI (electron channelling contrast imaging) technique. EBSD-measurements were performed in order to analyze the phase transformations of the TRIP/TWIP steels using HKL-technology from Oxford Instruments.

3. Results

3.1. Initial microstructure and tensile properties

Both austenitic steels are characterized by a dendritic cast microstructure, which is exemplarily shown in Fig. 1 (a) for the alloy 16-7-8, with a few annealing twins and small amounts of MnS and δ-ferrite. The grain sizes, determined by the linear intercept method, are in the range of 160-740 µm. The technical tensile stress-strain curves are plotted in Fig. 1 (b) and the mechanical properties are summarized in Table 2.

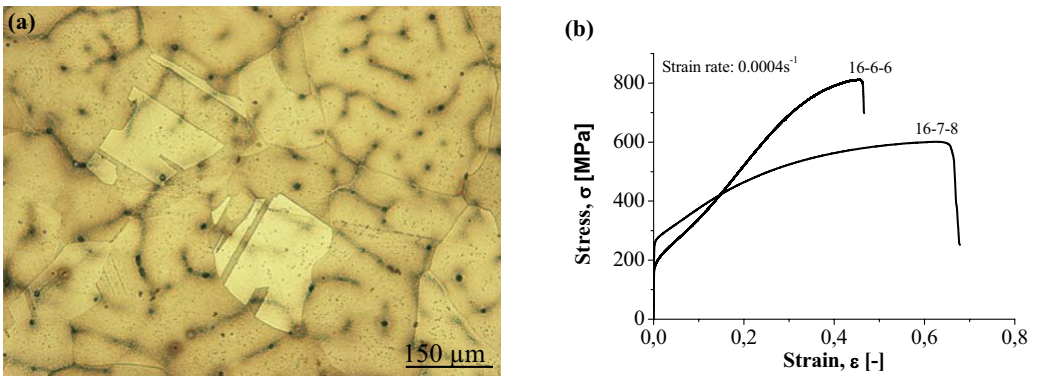

Fig. 1. (a) Optical micrograph of the steel 16-7-8 in the as heat-treated condition. (b) Technical tensile stress-strain curves of the investigated steels.

The ductility increases with a rising nickel and manganese content, whereas the work hardening capacity decreases. This behavior is caused by the higher austenite stability of the steel 16-7-8, resulting in a lower fraction of deformation-induced α'-martensite. In the stress-strain curve of the steel 16-6-6 two inflection points can be observed, but the alloy 16-7-8 shows none. According to Weiß et al. [28] inflection points in the stress-strain curve indicate that

the deformation-induced α'-martensite fraction exceeds 20 %. Consequently, the steel 16-7-8 is characterized by other work hardening mechanisms, e.g. deformation-induced formation of twins, stacking faults and/or ε-martensite.

3.2. Low cycle fatigue behavior

The variation of the stress amplitudes (Δσ/2) with number of cycles (N) is presented in Fig. 2 for the investigated strain amplitudes ($\Delta\varepsilon_t/2$). The cyclic stress response for the two studied cast steels is completely different. Concerning the steel 16-7-8, the cyclic stress response can be generally classified into the following three cases depending on the applied total strain amplitude. (i) At low strain amplitudes ($\Delta\varepsilon_t/2 < 0.8\cdot10^{-2}$) an initial hardening followed by a small amount of softening and almost stable stress response can be observed. (ii) Intermediate strain amplitudes ($0.8\cdot10^{-2} < \Delta\varepsilon_t/2 < 1.4\cdot10^{-2}$) result in a comparable behavior with an additional secondary hardening. (iii) At larger strain amplitudes $\Delta\varepsilon_t/2 \geq 1.4\cdot10^{-2}$ the cyclic stress response revealed very rapid strain hardening without reaching a level of saturation until the final fracture.

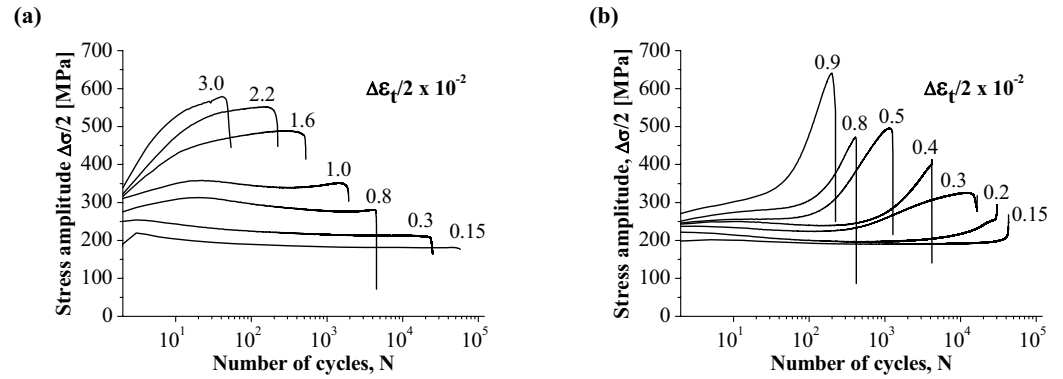

Fig. 2. Cyclic deformation curves of the investigated cast TRIP/TWIP steels. (a) Steel 16-7-8, (b) steel 16-6-6.

Regarding the steel 16-6-6, it can be observed that almost no primary hardening occurs. The "secondary" hardening starts already at low strain amplitudes ($\Delta\varepsilon_t/2 \geq 0.2\cdot10^{-2}$), Fig. 2 (b). Moreover, this "secondary" hardening increases with increasing strain amplitudes and the onset is shifted to lower number of cycles. This kind of hardening was also observed in other metastable austenitic steels, such as AISI 304L and 201 [13,22,24], and is an indicator for an occurring martensitic transformation.

Table 2 Monotonic and cyclic mechanical properties of the cast TRIP/TWIP steels compared to other austenitic steels.

Monotonic	16-6-6	16-7-8	AISI 201[22]	AISI 202 [22]
Young's modulus, E [GPa]	191	191	193	193
0.2 % yield strength, σ_{ys} [MPa]	186	263	324	359
Ultimate tensile strength, σ_{UTS} [MPa]	792	594	974	698
Elongation at fracture, A [%]	43.8	63	-	-
Fatigue				
Fatigue strength coefficient, σ'_f [MPa]	2144	2312	-	3184
Fatigue strength exponent, b	-0.18	-0.21	-	-0.23
Fatigue ductility coefficient, ε'_f	0.09	0.44	-	0.278
Fatigue ductility exponent, c	-0.45	-0.52	-	-0.43

The martensite formation curves of the steel 16-6-6 are shown in Fig. 3 (a) and support definitely that the α'-martensite formation is responsible for the observed hardening. The evolution of the α'-martensite content exhibits an incubation period, which becomes shorter with increasing strain amplitude. A pronounced martensitic phase transformation starts at a total strain amplitude of $\Delta\varepsilon_t/2 \geq 0.2 \cdot 10^{-2}$. At lower strain amplitudes only at a few places some α'-martensite nuclei were detected. Additional measurements with a magnetic balance confirm the results of the feritscope measurements and thus verify the conversion factor of 1.7, stated by Talonen et al. [27]. The deviations are caused by differences in the crystallographic orientation and in the local chemical composition resulting in a very heterogeneous distribution of the α'-martensite in the cast material, as shown in Fig. 3 (b). Whereas the grains I and III are unfavorably oriented to the load axis causing a low amount of α'-martensite, grain II is almost completely transformed since it contains a primary slip system oriented at 45° to the load axis. Conversely, the steel 16-7-8 shows a maximum α'-martensite content of only ~ 5% at a total strain amplitude of $3 \cdot 10^{-2}$ which is caused by the high stability of the austenitic phase [23].

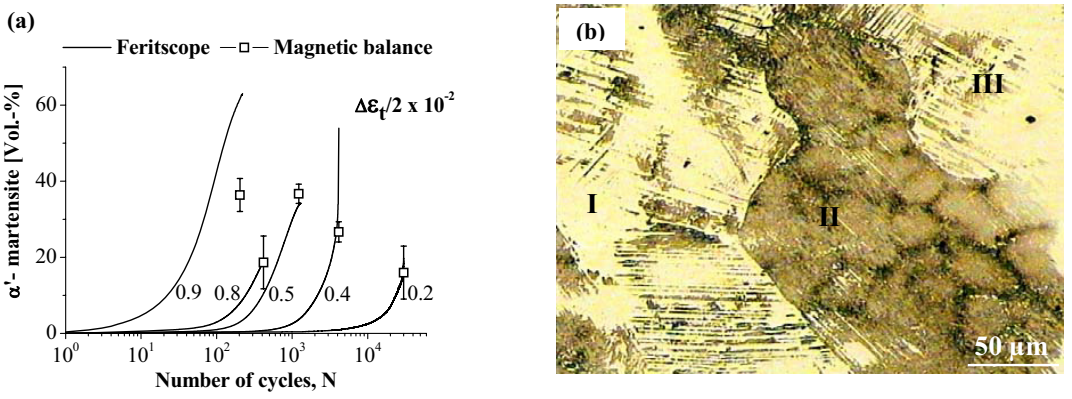

Fig. 3. (a) Cyclic martensite formation curves of the steel 16-6-6. (b) Optical micrograph (color etching) showing the α'-martensite formation (dark brown) in differently oriented grains. The specimen was deformed with $\Delta\varepsilon_t/2 = 0.4 \cdot 10^{-2}$ and the micrograph was taken at N_f. Load axis is vertical.

The fatigue lives of both cast steels follow the strain–life relationship proposed by Basquin and Manson-Coffin, which is given by:

$$\Delta\varepsilon_t / 2 = \Delta\varepsilon_e / 2 + \Delta\varepsilon_p / 2 = \frac{\sigma_f'}{E}\left(2N_f\right)^b + \varepsilon_f'\left(2N_f\right)^c \quad (4)$$

where $\Delta\varepsilon_e/2$ and $\Delta\varepsilon_p/2$ are the elastic and plastic strain amplitudes at the half life time, σ'_f the fatigue strength coefficient, b the fatigue strength exponent, ε'_f the fatigue ductility coefficient, c the fatigue ductility exponent and E the Young's modulus, respectively. The values of $\Delta\varepsilon_e/2$ and $\Delta\varepsilon_p/2$ were determined by measuring the width of the hysteresis loops at the mean stress. The application of Hook`s law to determine the elastic and plastic strain amplitudes resulted in quite different parameters [23] since the stiffness of the specimens altered during cycling.

The fatigue lives of the cast steels are plotted in Fig. 4 (a) and the parameters of both materials are summarized in Table 2. In both cases, the wide scatter is caused by the inhomogeneous cast structure with stress concentrations, e.g. micropores, and segregations. It becomes evident that the cast steel 16-7-8 exhibits higher fatigue lives at strain amplitudes larger than $2 \cdot 10^{-3}$. Conversely, at lower strain amplitudes the fatigue life of 16-6-6 is superior. The ratio of fatigue lives of the investigated materials is reduced from a factor of ~10 at a strain amplitude of $1 \cdot 10^{-2}$ to ~0.5 at $1 \cdot 10^{-3}$. This crossover of the fatigue curves of the more metastable steel over the stable material was also observed by Franke et al. [22] and Hennessy et al. [26] and was explained by the beneficial effects of the α'-martensite formation at low strain amplitudes.

Fig. 4 (b) shows the fatigue life curves of the two cast steels compared to the austenitic steels AISI 201 and AISI 202. Depending on the austentite stability a rotation of the fatigue life curves occurs. The more metastable steels (16-6-6 and AISI 201) exhibit a lower slope, resulting in reduced fatigue lives in the LCF-regime and higher fatigue lives in the HCF regime, respectively. Conversely, as a result of the high ductility the more stable steels (16-7-8 and AISI 202) show higher fatigue lives at higher strain amplitudes.
The disadvantageous effect of the α'-martensite formation at high strain amplitudes and the beneficial effect at low strain amplitudes can be explained by the pronounced hardening which is caused by the α'-martensite formation. The cyclic hardening leads in strain controlled tests to a fatigue life reduction in the LCF regime. However, in the HCF regime a local transformation of austenite into α'-martensite results in a fatigue life improvement since the dislocation movement in these transformed areas is constrained.

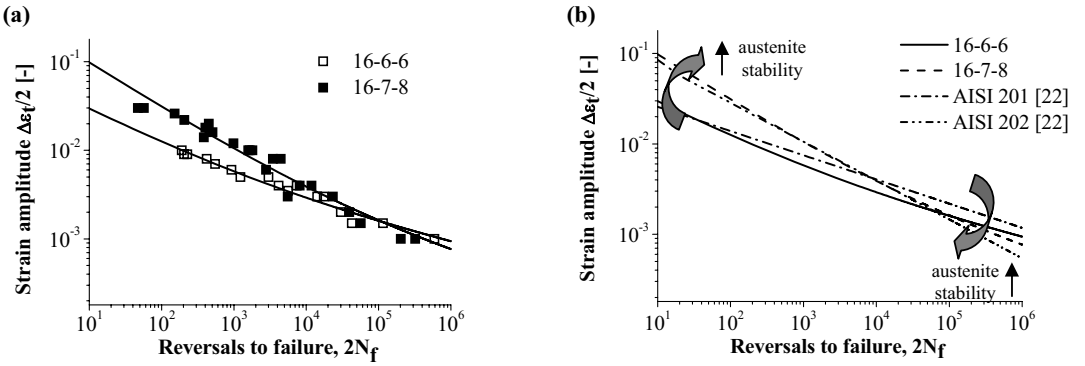

Fig. 4. (a) Fatigue life curves of the investigated cast steels. (b) Comparison of fatigue life curves of different austenitic steels with variations in austenite stability.

3.3. Deformation microstructures

In Fig. 5 selected deformation microstructures are shown. In both cast steels the microstructure is characterized by deformation bands, whose density and thickness increases with increasing strain amplitudes.

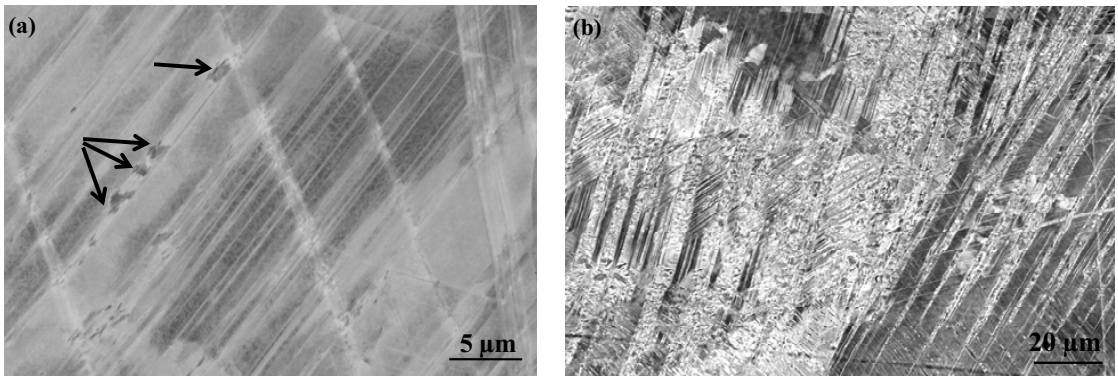

Fig. 5. SEM micrographs (BSE) depicting the deformation microstructures and locations of the phase transformations inside the deformation bands. (a) Steel 16-7-8 deformed at $\Delta\varepsilon_t/2 = 1.2 \cdot 10^{-2}$. (b) Steel 16-6-6 deformed at $\Delta\varepsilon_t/2 = 0.3 \cdot 10^{-2}$. Load axis is horizontal, the samples were deformed to failure.

The grains show different activated slip systems as a result of the distinct crystallographic orientation and Schmid factor. As well known, grains oriented 45° to the load axis start to deform first. The α'-martensite nucleation occurs at the intersections of these deformation bands and in the volume, as already observed by Martin et al. [29] at monotonic deformation of a comparable cast steel. Whereas in the steel 16-6-6 the deformation bands show a high amount of α'-martensite, in the steel 16-7-8 the transformation happens only at a few places which is caused by the higher austenite stability. The morphology of the α'-martensite inside the deformation bands can be described as lenticular. Fig. 6 presents the EBSD maps showing the phases and orientations in the deformed microstructures of the steel 16-7-8. It becomes evident that the darker areas marked in Fig. 5 (a) with black arrows are indexed as the bcc α'-martensite phase (blue color). The intermediate ε-martensite phase was not detected. Inside the deformation bands the amount of zero solutions is always higher than in the austenitic matrix which is caused by the increased defect density inside these bands. Moreover, the boundaries of the matrix and the deformation bands are often characteristical twin boundaries (Σ3, marked with yellow color in Fig. 6 (b)). These boundaries are characterized by a rotation of 60° around an <111> axis leading to an orientation change in the austenitic phase, as shown in Fig. 6 (b) by green color inside the deformation bands and pink color for the matrix. Thus, the steel 16-7-8 can be classified into the group of TWIP-steels, which is supported by the higher SFE.

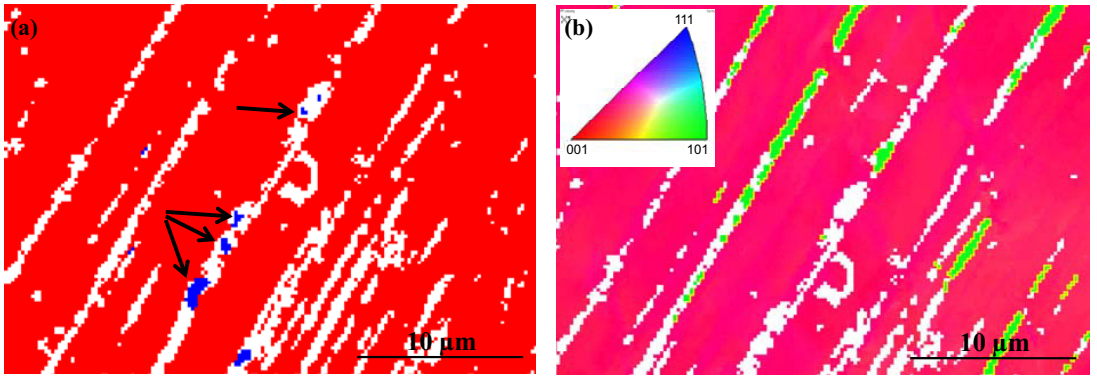

Fig.6: EBSD maps of the steel 16-7-8 deformed to failure at $\Delta\varepsilon_t/2 = 1.2 \cdot 10^{-2}$. (a) EBSD-phase map – red color fcc, blue color bcc. (b) EBSD-orientation map, colors with respect to the stereographic triangle given in the left upper corner. Zero solutions are indexed by white color. Load axis is horizontal.

Inside the deformation bands of the steel 16-6-6 small amounts of hexagonally indexed regions, called in the following ε-martensite, can be found and the majority consists of α'-martensite (Fig. 7 (a)). Martin et al. [29] as well as Weidner et al. [30] found that only deformation bands which exceed a certain width can be indexed with the dataset of the hexagonal ε-martensite phase. On the other hand, thin deformation bands are mostly indexed as fcc. Both authors stated that this phenomenon is closely related to the density of stacking faults, which increases with increasing width of the deformation bands. If a stacking fault appears on every second {111} plane of the austenite, the structure of hexagonal ε-martensite is formed. Obviously, with increasing thickness of the deformation bands the probability for this sequence increases too, resulting in more hexagonal phase, as shown in the EBSD map in Fig. 7 (a). Therefore, under cyclic loading the transformation from austenite to α'-martensite occurs via the intermediate hexagonal phase, as also observed in other austenitic steels [13,26]. Since the specimens were deformed until failure the main part of this hexagonal material was finally transformed into α'-martensite.

Additional support of the EBSD measurements was obtained by XRD analyses. Fig. 7 (b) shows the X-ray diffraction results of the materials after fatigue testing. The steel 16-7-8 subjected to $\Delta\varepsilon_t/2 = 1.2 \cdot 10^{-2}$ contains only austenite. However, diffraction patterns of the steel 16-6-6 show peaks indicating ε-martensite and α'-martensite. It is important to note that as a result of the coarse grained material the XRD analyses allow only to obtain qualitative information since only some diffraction peaks can be observed, depending on the orientation of the examined grains.

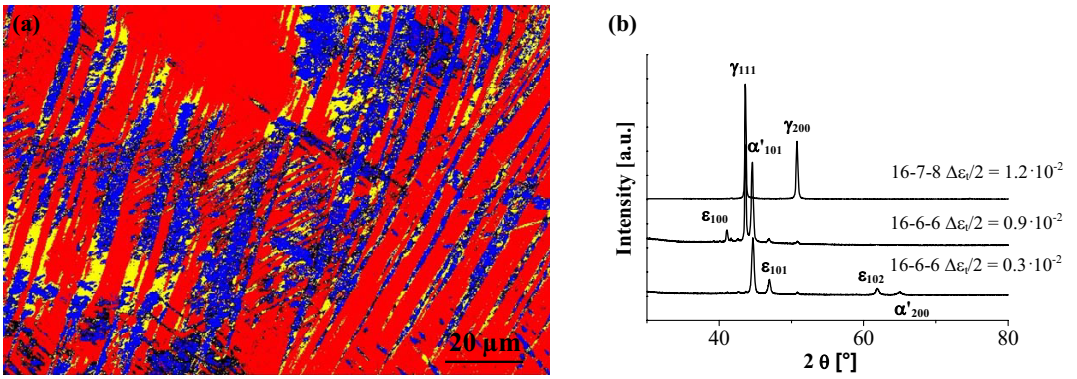

Fig.7. (a) EBSD-phase map of the steel 16-6-6 deformed to failure at $\Delta\varepsilon_t/2 = 0.9 \cdot 10^{-2}$. Red color fcc (γ), blue color bcc (□□) and yellow color hcp (ε). Load axis is horizontal. (b) XRD patterns of deformed specimens.

ECC-images were taken in order to analyze the developed dislocation structures. As observed in a former study [23], the steel 16-7-8 is characterized by planar dislocation structures at low strain amplitudes and cell/wall structures at increased strain amplitudes. Fig. 8 (a) represents exemplarily the cellular dislocation structure which has been developed in the steel 16-7-8 at $\Delta\varepsilon_t/2 = 1.2 \cdot 10^{-2}$. The deformation bands consist of very fine lamellas which can be correlated with the formation of stacking faults and micro twins. These findings are in agreement with those of other authors who have observed similar deformation microstructures in austenitic steels with a low SFE [31-33]. It is stated [33] that the stacking faults between partial dislocations become larger with increasing deformation resulting finally in stacking faults which cover whole grains. With increasing density of stacking faults the faulted regions on adjacent glide planes began to overlap or gliding of partial dislocations on successive planes occurs leading to the formation of twin bands which is supported by the observed twin boundaries shown in Fig. 6 (b).

An ECC image around a crack tip of the 16-6-6 specimen is shown in Fig. 8 (b). Near the crack tip the deformed steel 16-6-6 shows a cell/wall dislocation structure. On the other hand, far from the fatigue crack planar glide is the prevalent mechanism [30]. This transition from planar to wavy dislocation structures as a result of the increasing plastic deformation, in this case in the crack tip plastic zone, is characteristic for fcc metals with a SFE around 20 mJ/m² [35]. Additionally, the lamellar structures as observed in the steel 16-7-8 can be seen as well.

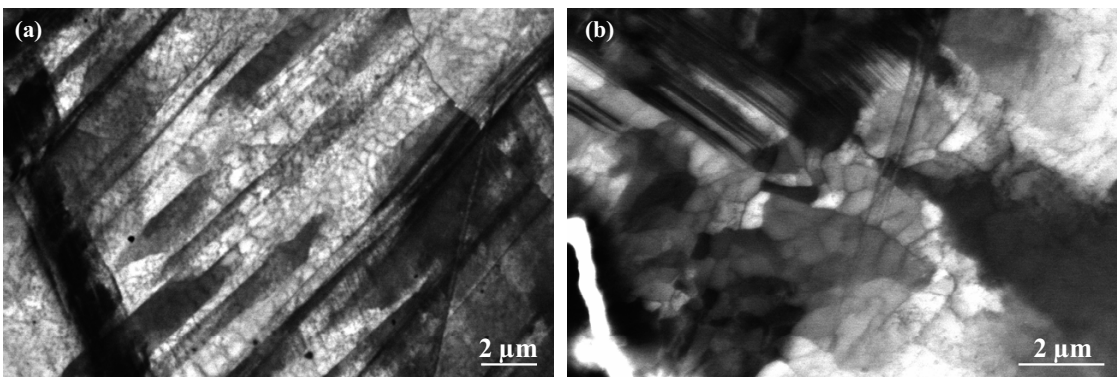

Fig.8. (a) ECC-images showing the dislocation structures of the deformed cast steels. (a) Well developed cell/wall dislocation structure in the steel 16-7-8 deformed at $\Delta\varepsilon_t/2 = 1.2 \cdot 10^{-2}$. (b) Planar dislocation structures in the volume and cell-arrangements near a fatigue crack obtained from the steel 16-6-6 deformed at $\Delta\varepsilon_t/2 = 0.3 \cdot 10^{-2}$. Load axis is horizontal.

4. Conclusions

In the present work the effect of the austenite stability on the low cycle fatigue behavior of high alloyed metastable austenitic cast steels has been investigated. The following conclusions can be drawn:

(1) With increasing austenite stability the fatigue life at high strain amplitudes (LCF) is improved. At low strain amplitudes (HCF) the local martensitic phase transformation of the steel with lower austenite stability leads to higher fatigue lives.
(2) The more metastable 16-6-6 shows a pronounced hardening at $\Delta\varepsilon_t/2 \geq 0.2 \cdot 10^{-2}$ which is caused by the α'-martensite formation. With increasing strain amplitudes the onset of the α'-martensite transformation is shifted to a lower value of the cumulative plastic strain.
(3) The α'-martensite transformation occurs inside the deformation bands via the intermediate ε-martensite phase which is formed by stacking faults on every second {111} plane of the austenitic phase.
(4) The cyclic hardening of the steel 16-7-8 at $\Delta\varepsilon_t/2 > 0.8 \cdot 10^{-2}$ results from the formation of deformation-induced twins and/or stacking faults and a small amount of α'-martensite.
(5) Both cast steels show a transition from planar to wavy dislocation structures with increasing plastic strain amplitude. Moreover, characteristical lamellas which are correlated with micro twins, stacking faults and ε-martensite were found.

Acknowledgements

The authors gratefully acknowledge the support of the German Research Foundation (DFG) within the Collaborative Research Center SFB 799. Special thanks go also to K. Zuber for the preparation of all specimens for microstructural investigations and to Dipl.-Wi.-Ing. S. Wolf and Dipl.-Ing. T. Richter for providing static stress-strain curves.

References

[1] A. Weiß, H. Gutte, M. Radke, P.R. Scheller, patent specification WO002008009722A1.

[2] A. Jahn, A. Kovalev, A. Weiß, P.R. Scheller, S. Wolf, L. Krüger, S. Martin, U. Martin: Mechanical properties of high alloyed cast and rolled CrMnNi TRIP steels varying Ni contents. In Proc. of ESOMAT 2009, eds. P. Sittner, L. Heller, V. Paidar, published by EDP Sciences (www.esomat.org), paper 05013, DOI:10.1051/esomat/200905013.

[3] A. Jahn, A. Weiß, P.R. Scheller: Stähle für höchste Beanspruchungen. Stahl und Eisen 2009; 129: 92-100.

[4] J. Charles: The new 200-series: An alternative answer to Ni surcharge? Dream or nightmare? Proc. of the Fifth Stainless Steel Science and Market Congress, (2005) (www.euro-inox.org 24.02.2010).

[5] A.S. Hamada, L.P. Karjalainen, J. Puustinen: Fatigue behavior of high-Mn TWIP steels. Mater. Sci. and Eng. A 2009; 517: 68-77.

[6] G. Frommeyer, U. Brüx, P. Neumann: Supra-Ductile and High-Strength Manganese-TRIP/TWIP Steels for High Energy Absorption Purposes. ISIJ Int. 2003; 43: 438-446.

[7] F. Pickering: Physical metallurgical development of stainless steels. Proc. Conf. Stainless Steels Göteborg (1984), The Institute of Metals, London (1985) p. 2.

[8] A.G. Pineau, R.M. Pelloux: Influence of Strain-induced Martensitic Transformations on Fatigue Crack Growth Rates in Stainless Steels. Met. Trans. 1974; 5A: 1103-1112.

[9] B. Cina: J. Iron Steel Inst. (1954) 791.

[10] G.B. Olson, M. Cohen: Kinetics of Strain-Induced Martensitic Nucleation. Met. Trans. A 1975; 6A: 791-795.

[11] W.J. Dan, S.H. Li, W.G. Zhang, Z.Q. Lin: The effect of strain-induced martensitic transformation on mechanical properties of TRIP steel. Materials & Design 2008; 29: 604-612.

[12] K.H. Lo, C.H. Shek, J.K.L. Lai: Recent developments in stainless steels. Mater. Sci. and Eng. R 2009; 65: 39-104.

[13] M. Bayerlein, H.-J. Christ, H. Mughrabi: Plasticity-induced martensitic transformation during cyclic deformation of AISI 304L stainless steel. Mater. Sci. and Eng. A 1989; 114: L11-L16.

[14] S.G. Hong, S.B. Lee, T.S. Byun: Temperature effect on the low-cycle fatigue behavior of type 316L stainless steel: Cyclic non-

stabilization and an invariable fatigue parameter. Mater. Sci. and Eng. A 2007; 457: 139-147.

[15] M. Bayerlein, H. Mughrabi, M. Kesten, B. Meier: Improvement of the strength of a metastable austenitic stainless steel by cyclic deformation-induced martensitic transformation at 103 K. Mater. Sci. and Eng. A 1992; 159: 35-41.

[16] J. Kaleta, G. Zicetek: Identification of cyclic softening and □-□ hysteresis in austenitic steel with plasticity-induced martensitic transformation. Mater. Sci. and Eng. A 1997; 234-236: 680-683.

[17] R.G. Teteruk, H.J. Maier, H.-J. Christ: Fatigue-induced martensitic transformation in metastable stainless steels. Low cycle fatigue and elasto-plastic behaviour of materials (1998); eds. K.-T. Rie und P.D. Portella, Elsevier Applied Science, 321-326.

[18] J. Kaleta, G. Zicetek: Representation of cyclic properties of austenitic steels with plasticity-induced martensitic transformation. Fatigue & Fracture of Engineering Materials & Structures 1998; 21: 955-964.

[19] M. Topic, R.B. Tait, C. Allen: The fatigue behaviour of metastable (AISI-304) austenitic stainless steel wires. Int. J. Fatigue 2007; 29: 656-665.

[20] M. Smaga, F. Walther, D. Eifler: Deformation-induced martensitic transformation in metastable austenitic steels. Mater. Sci. and Eng. A 2008; 483-484: 394-397.

[21] M. Grosse, D. Kalkhof, M. Niffenegger, L.Keller: Influencing parameters on martensite transformation during low cycle fatigue for steel AISI 321. Mater. Sci. and Eng. A 2006; 437: 109-113.

[22] G. Franke, C. Altstetter: Low-Cycle Fatigue Behavior of Mn/N Stainless Steels. Met. Trans. A 1976; 7a: 1719-1727.

[23] A. Glage, A. Weidner, T. Richter, P. Trubitz, H. Biermann: Low cycle fatigue behavior and microstructure of a high alloyed metastable austenitic cast TRIP-steel. In Proc. of ESOMAT 2009, eds. P. Sittner, L. Heller, V. Paidar, published by EDP Sciences (www.esomat.org), paper 05007, DOI:10.1051/esomat/200905007.

[24] U. Krupp, C. West, H. -J. Christ: Deformation-induced martensite formation during cyclic deformation of metastable austenitic steel: Influence of temperature and carbon content. Mater. Sci. and Eng. A 2008; 481-482: 713-717.

[25] G. Baudry, A. Pineau: Influence of strain-induced martensitic transformation on the low-cycle fatigue behavior of a stainless steel. Mater. Sci. and Eng. 1977; 28: 229-242.

[26] D. Hennessy, G. Steckel, C. Altstetter: Phase transformation of stainless steel during fatigue. Met. Trans. A 1976; 7A: 415-424.

[27] J. Talonen, P. Aspegren and H. Hänninen: Comparison of different methods for measuring strain induced □'-martensite content in austenitic steels. Mater. Sci. and Technol. 2004; 20: 1506-1512.

[28] A. Weiß, H. Gutte, P.R. Scheller: Deformation-induced martensite formation in the metastable austenitic steel X5CrNi18-10 (1.4301, AISI 304) and transformation induced plasticity. Proc. of the Fifth Stainless Steel Science and Market Congress, (2005).

[29] S. Martin, S. Wolf, U. Martin, L. Krüger, A. Jahn: Investigations on martensite formation in CrMnNi-TRIP steels. In Proc. of ESOMAT 2009, eds. P. Sittner, L. Heller, V. Paidar, published by EDP Sciences (www.esomat.org), paper 05022, DOI:10.1051/esomat/200905022.

[30] A. Weidner, A. Glage, H. Biermann: In-situ Characterization of the Microstructure Evolution during Cyclic Deformation of Novel TRIP Steel. Proc. of Fatigue conference 2010, Prague, Procedia Engineering; 2010.

[31] D. Ye, S. Matsuoka, N. Nagashima, N. Suzuki: The low-cycle fatigue, deformation and final fracture behaviour of an austenitic stainless steel. Mater. Sci. and Eng. A 2006; 415: 104-117.

[32] M. Botshekan, J. Polák, Y. Desplanques, S. Degallaix: Low-cycle fatigue behaviour of a 316LN stainless steel at 77 K and associated structural transformation. Low cycle fatigue and elasto-plastic behaviour of materials (1998); eds. K.-T. Rie und P.D. Portella, Elsevier Applied Science, 309-314.

[33] T.S. Byun, E.H. Lee, J.D. Hunn: Plastic deformation in 316LN stainless steel-characterization of deformation microstructures. J. Nucl. Mater. 2003; 321: 29-39.

[34] T. Kruml, J. Polák, K. Obrtlik, S. Degallaix: Dislocation structures in the bands of localised cyclic plastic strain in austenitic 316L and austenitic-ferritic duplex stainless steels. Acta Metallurgica 1997; 45: 5145-5151.